Welding in the World (2019) 63:23–31
https://doi.org/10.1007/s40194-018-0641-3

RESEARCH PAPER

Numerical investigations on the thermal efficiency in laser-assisted plasma arc welding

S. Jäckel[1] · M. Trautmann[1] · M. Hertel[1] · U. Füssel[1] · D. Hipp[1] · A. Mahrle[2] · E. Beyer[1,2]

Received: 7 August 2017 / Accepted: 20 August 2018 / Published online: 27 August 2018

Abstract
Numerical investigations on the thermal efficiency in laser-assisted plasma arc welding (LAPAW) have been carried out by the combination of a magneto-hydrodynamic (MHD) arc model and a smoothed-particle-hydrodynamics (SPH) model of the weld pool. The comparison of the calculated weld seam cross-sections gained from numerical simulation as well as experimental examinations shows a good agreement. By the use of the weld pool model, the sensitivity of different influencing variables was investigated. The analysis clearly reveals the major influence of the central heat flux density on the penetration profile and on the thermal efficiency of the process. The higher the heat flux of the laser beam and the higher the constriction of the heat flux profile of the arc, the higher the thermal efficiency of the process.

Keywords Laser-enhanced plasma welding · Hybrid laser arc welding · Plasma welding · Plasma · Laser-arc interaction · Hybrid · Molten pool · Simulating

1 Introduction

Arc welding processes are established and frequently used technologies for joining a variety of different materials. In order to increase the applicability and efficiency of welding processes, combinations of arc and laser welding processes increasingly gain interest in both scientific investigations as well as industrial applications. By combining these processes, disadvantages of the processes should be compensated and synergy effects can be created.

State of the art is the use of hybrid welding processes with a comparable heat input from the laser and the arc welding process. The process was first investigated by Steen and Ebo [1] as well as Steen [2]. Based on experimental investigations, it was found that the arc attachment is highly influenced by the laser-generated hot spot at the parent material surface. Due to a constricted arc root, the usage of a laser-TIG hybrid welding process enables an increased welding speed as well as increased penetration depths compared to individual and subsequently applied laser beam and TIG-welding processes.

In contrast, laser-assisted arc welding processes are based on the primary heat input into the workpiece by the welding arc. The laser beam serves only as a minor secondary heat source. By additionally using a laser with a comparatively low power, the stability of the arc can be considerably increased [3–6]. In addition, the penetration depth and the welding speed can be increased significantly [7–14]. Several scientific studies have been carried out to get a closer insight in the physics of the synergy effect in laser-assisted arc welding.

Cui et al. [7] and Decker et al. [8] used a CO_2 laser (λ_{CO2} = 10.6 μm) to investigate the synergy effect in laser assisted gas tungsten arc welding. It was found that the penetration and the welding speed can be increased considerably by means of a laser with a power of only 100 W. The authors stated that the investigated effect is based on an increased current density of the welding arc as well as an enhanced laser beam absorption on the workpiece surface.

Decker et al. [8] and Mahrle et al. [9] both assume that the properties of the welding arc are not directly influenced by the laser radiation but indirectly by a laser-induced evaporation of the base material. Because the ionisation potential of the produced metal vapour is comparatively low compared to the

Recommended for publication by Commission XII - Arc Welding Processes and Production Systems

✉ S. Jäckel
sebastian.jaeckel@tu-dresden.de

[1] Technische Universität Dresden, 01062 Dresden, Germany

[2] Fraunhofer Institute of Material and Beam Technology, Winterbergstraße 28, 01277 Dresden, Germany

shielding gas components used in gas tungsten arc welding (GTAW) and plasma arc welding (PAW), the electrical conductivity of the plasma increases as a result of a slight evaporation. The increased electrical conductivity leads to a contraction of the anodic arc root and thus to an enhanced current density at the base material surface. In contrast, high amounts of metal vapour have a contrary effect. Because of a significantly increased radiative emission of the evaporated metal vapour, a minimum of the temperature and thus decreased current densities are caused in the arc core. In addition, Mahrle et al. [9] conclude that enhanced heat flow conditions inside the base material can have a major impact on the synergy effect as well.

Hu and Ouden [10] investigated the synergy effect between a GTAW welding process and a Nd:YAG laser with a power of 500 W. They stated that the melting efficiency is increased as a result of an increased current density. In contrast to the argumentations of Decker and Mahrle, the increase of the current density is not explained by an evaporation effect but by the superpositioning of different heat sources as well as the contraction of the welding arc due to the laser radiation.

Mahrle et al. [11, 12] and Rose et al. [13] performed experimental investigations on the interaction between a plasma welding process and a single-mode fibre laser (λ_{Yb} = 1.07 μm) in a coaxial setup. The process is referred to as laser-assisted plasma arc welding (LAPAW). By shifting the laser radiation inside a hollow cathode, the authors concluded that the position of the beam spot has a crucial impact on the performance and characteristic of the process (see Fig. 1).

It is consequently assumed that the synergy effect is mainly driven not by a direct interaction between the welding arc and the laser beam but by indirect interactions at the workpiece surface. Besides the effect of evaporation of the base material, the authors assume that the synergy effect is also driven first by an enhanced absorption of the laser beam due to the preheating of the workpiece surface and second by changed flow conditions inside the weld pool.

In summary, it can be concluded that the synergy effect in laser-assisted arc welding is explained in the literature mainly by three possible driving effects: First, the absorption of the laser beam by the base material is raised significantly due to the preheating of the workpiece surface by the plasma arc. Second, laser-induced evaporation leads to an increased electrical conductivity in the arc plasma and thus to higher current densities and heat fluxes of the welding arc at the base material surface. Third, additional heating of the weld pool by the laser beam possibly leads to altered thermal boundary conditions resulting in changed flow conditions inside the weld pool.

It can be assumed that the synergy effect is caused by a super positioning of several physical processes (e.g. a higher heat flux density at the weld pool surface or an intensified flow field in the weld pool). For this reason, the aim of this paper is not to analyse different process parameters but the influence of different driving forces. In the future, this will allow the synergy effect to be enhanced by increasing beneficial driving forces and reducing compensating driving forces.

In contrast to experimental investigations, the application of numerical methods enables the separation of influencing factors and thus the purposeful analysis of major effects without changing other boundary conditions. For the described process analysis established numerical models for the arc [14–16] and the weld pool [17–19]. A detailed description of the models is not included in this paper as they are described in detail in the literature. In order to analyse the mentioned synergy effects, we changed the absorption of the laser as well as the heat flux density profile, the shear stress profile and the pressure profile of the arc at the base material surface.

2 Methodical approach

The investigations were carried out using numerical models in order to calculate both the properties of the welding arc as well as the resulting weld pool formation.

By the application of a magnetohydrodynamic (MHD) model of the welding arc, the heat flux density $\dot{\boldsymbol{q}}$, the shear stress $\boldsymbol{\tau}$ as well as the pressure $\boldsymbol{p}$ at the workpiece surface are gained for a plasma welding process with a hollow cathode (Fig. 2). The discretization of the computational domain is based on the experimental setup by Rose et al. [13] taking into account all geometries influencing the fluid flow in the process region. A steady-state calculation was performed using an axis symmetric model and temperature-dependent plasma properties from Murphy [20]. A detailed model description could be found by Schnick et al. [16].

In the calculation an arc current of 50 A, a plasma gas nozzle diameter of 1.6 mm, a plasma gas volume flow rate of 0.6 l min^{-1}, a distance between the bottom of the plasma gas nozzle and the workpiece surface (working distance) of 5 mm and a shielding gas volume flow rate of 20 l min^{-1} were used. The plasma gas as well as the shielding gas was defined to be pure argon.

In order to analyse the weld pool formation, an incompressible smoothed particle hydrodynamics model (SPH) was used. The model takes into account the heat fluxes of the welding arc and the laser beam, the shear stress and pressure induced by the welding arc as well as Marangoni convection and the influence of the gravitation in the melt pool. The influences of the laser as well as the welding arc are approximated by source terms in the energy and momentum conservation equation. The approximations concerning the arc properties at the base material surface were derived from the MHD-model. The heat flux profile of the laser $\dot{\boldsymbol{q}}_{\boldsymbol{Laser}}$ at the base material surface was modelled in a simplified form by defining a heat source with a spot diameter of 500 μm and a uniform intensity distribution.

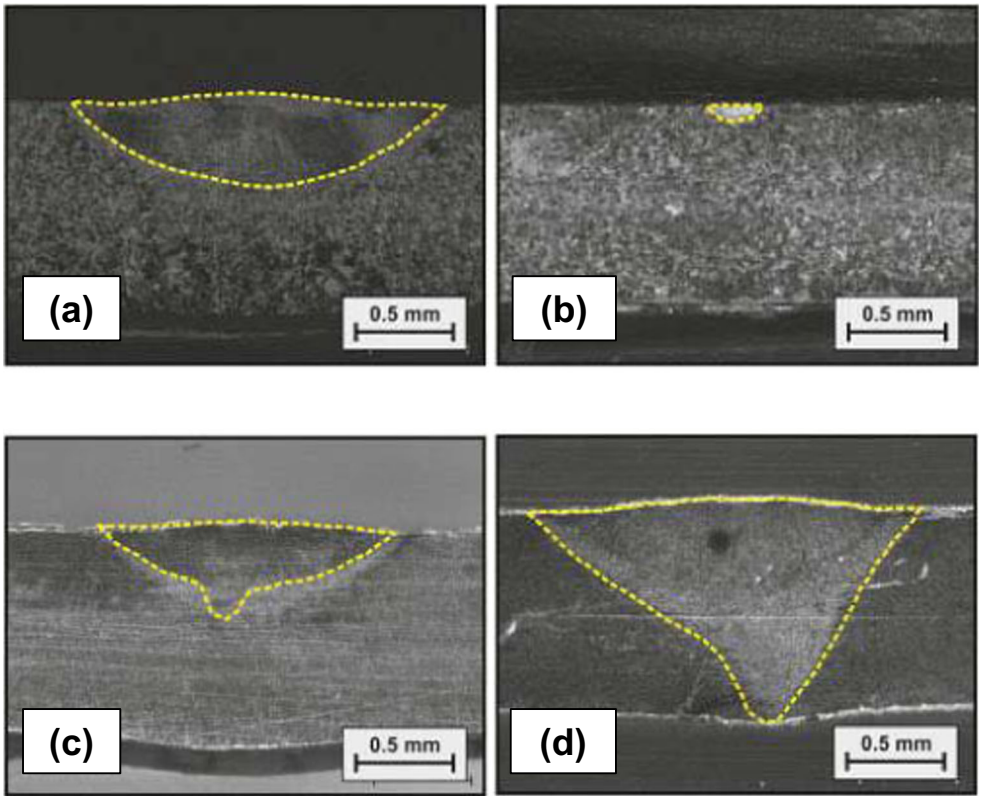

Fig. 1 Weld seam cross-sections for **a** PAW, **b** LBW, **c** LAPAW with leading laser position (**d**) LAPAW with trailing laser position on AISI 304 stainless steel [11]

All numerical calculations were done for a coaxial setup of the laser and the arc with an inclination angle of the torch of 90° and by assuming a constant absorption rate of the laser at the base material surface of 30%. Based on investigations from Cho et al. [21] and Kozakov et al. [22], interactions between the laser beam (Nd:YAG laser with a wavelength of 1.07 μm) and the arc column are neglectable and therefore not considered in the arc model. A detailed description of the weld pool model including all governing equations as well as boundary conditions could be found in Trautmann et al. [19]. The three-dimensional computational domain is discretized by approximately one million particles with a particle distance of about 0.075 mm (see Fig. 3).

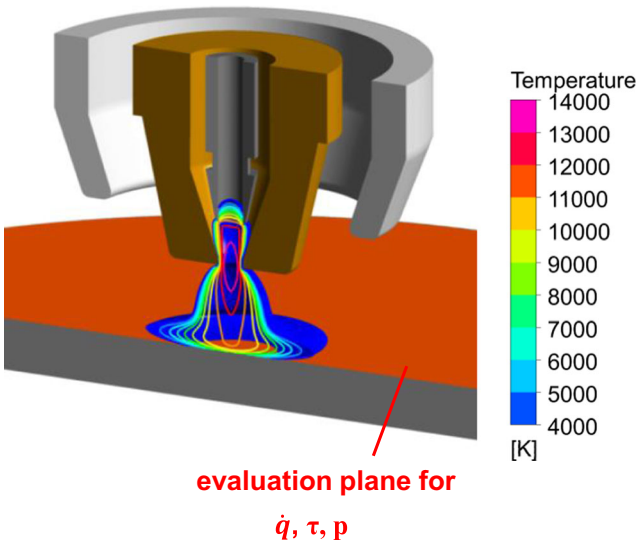

Fig. 2 MHD-model of the PAW process including the torch design with the hollow cathode

The calculations were carried out for AISI 304 stainless steel. The temperature-dependent density, specific heat and viscosity were set according to Radaj [23] with modifications for the mushy zone from Trautmann et al. [19]. The surface tension was set according to investigations of Fujii et al. [24]. Due to the significant influence of the thermal conductivity on the weld pool formation and the fact that there are significant differences in literature, a constant value of 20 W/m/K was assumed.

The influencing factors on the synergy effect in LAPAW are evaluated by the resulting cross-sections as well as the thermal efficiency, which is defined as the ratio between the required heat in order to form the weld and the heat induced by the welding arc and laser beam into the base material.

$$\eta_{th} = \frac{v_s \cdot A_s \cdot \rho \cdot \Delta h_{FZ}}{P_A + \alpha \cdot P_L} \tag{1}$$

In this relation, $\boldsymbol{v_S}$ is the travel speed, $\boldsymbol{A_s}$ is the area of the cross-section, $\boldsymbol{\rho}$ is the density at 300 K, $\boldsymbol{\Delta h_{FZ}}$ is the required increase of the specific enthalpy to cause heating of the material from 300 K to the meling point at 1750 K, $\boldsymbol{P_a}$ is the heat input of the arc, α is the absorptivity and $\boldsymbol{P_L}$ is the heat input of the laser.

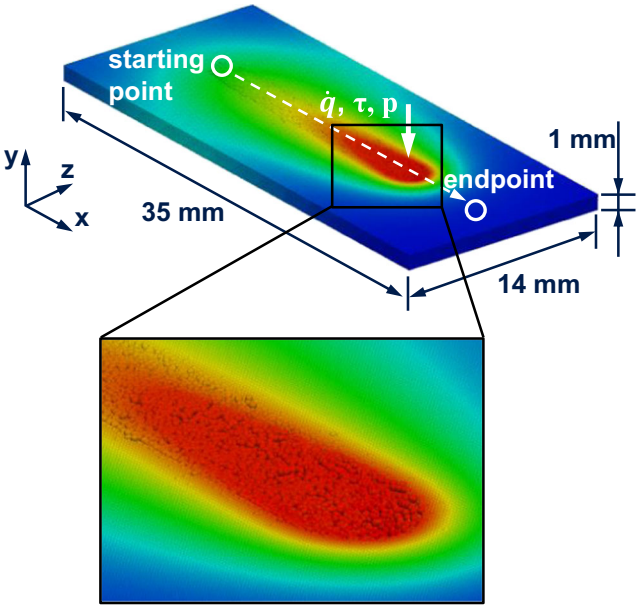

Fig. 3 Discretized geometry and basic procedure of the SPH calculations

3 Calculated arc properties at the base material surface and validation

Due to the geometry of the hollow cathode, the maximum temperature of approximately 13,900 K is not reached right under the tungsten cathode but at the outlet of the plasma gas nozzle. There are high plasma velocities occurring, which are caused by the geometric constriction of the arc and the thermal expansion of the gas induced due to the high plasma temperatures. The maximum velocity of approximately 380 m/s occurs below the bottom of the plasma gas nozzle. Figure 4 illustrates the calculated heat flux density $\dot{q}$, shear stress τ and pressure p evaluated at the workpiece surface.

Compared to GTAW, the geometric constriction of the arc leads to an increased heat flux density as well as higher shear stresses and a higher arc pressure at comparatively low welding currents. In total, a heat flow of approximately 500 W is induced into the base material by the welding arc under the described boundary conditions. The methodical approach is validated by a comparison of experimental determined and numerical calculated cross-sections for both the PAW and the LAPAW-process (see Fig. 5). By using the previously describes approach, the shape, width and depth of the weld pool of the PAW as well as the LAPAW-process can be predicted very well. The calculated cross-section of the LAPAW is slightly overestimated, which could be addressed to simplifications in the numerical models like the neglected evaporation, the constant absorption of the laser and the thermal conductivity of the base material. Nevertheless, the methodical approach is suitable for further investigations aiming to reveal the sensitivity of different process parameters on the synergy effect in LAPAW.

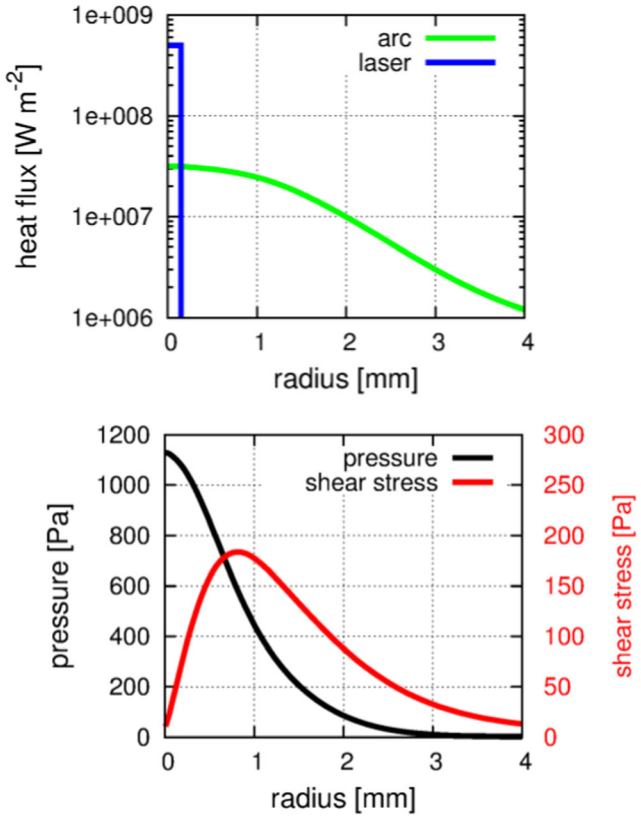

Fig. 4 Calculated profiles of the heat flux $\dot{q}$, shear stress τ and pressure p of the welding arcgained from the MHD model as well as the heat flux profile of the laser $\dot{q}_{Laser}$

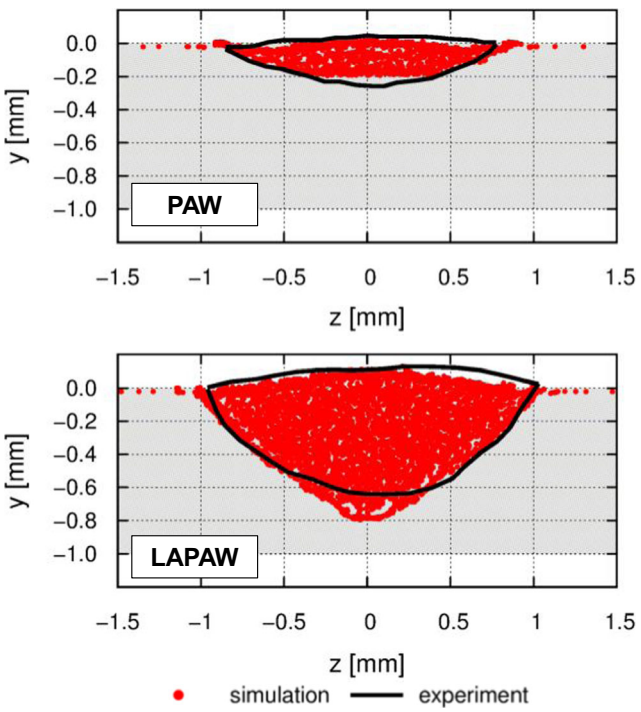

Fig. 5 Comparison of the cross-sections gained from numerical simulation (red) and experiments (black line) for the PAW (top) as well as the LAPAW process

4 Weld pool formation in laser-assisted plasma arc welding

Figure 6 shows the calculated temperature distributions in the weld pool for a PAW process as well as a LAPAW process with a laser power of 100 W, an absorptivity of about 30% and a travel speed of 0.7 m/min. In the calculations, the maximum temperature in the weld pool rises from 1820 to 2212 K due to the additional heat input by the laser beam. Because of the low thermal conductivity of AISI 304, the additional heat is efficiently used for melting the base material.

In comparison to PAW, the penetration in LAPAW can be enhanced significantly from 0.43 to 1 mm (weld through), whereas the weld pool width increased slightly from 2.26 to 2.48 mm. Consequently, the aspect ratio (ratio between penetration depth and weld pool width) in LAPAW increases as well. Furthermore, the weld seam cross-section is significantly enlarged from 0.65 to 1.57 mm^2.

Figure 7 shows the calculated velocity field in the weld pool. The arc-induced forces have a major impact on the flow characteristics of the weld pool and thus on the resulting weld seam formation. The heated melt is pushed to the back as well as to the side of the weld pool, leading to a flow directed to the rear part. From the back of the weld pool, the flow field is redirected to the process area. The backflow takes place at the bottom of the weld pool. The maximum velocity inside the weld pool increases from about 0.15 m/s (PAW) to 0.25 m/s (LAPAW), which can be attributed to the increased temperatures and thus to a reduced local density and a reduced local viscosity.

The high shear stress as well as the high pressure of the arc causes a significant deformation of the weld pool surface (see Fig. 8). Because of the enlarged weld pool volume, the effect is more pronounced in the case of the LAPAW process.

5 Sensitive analysis of different influencing variables

In order to analyse the influencing variables of the synergy effect in LAPAW, various sensitive analyses with the weld pool model were carried out. First, the influence of a possibly increased laser absorptivity of the base material due to a preheating by the arc is discussed. In order to analyse this effect, two different absorption rates of 50% and 100% at a constant laser power of 100 W (net laser heat input of 50 W and 100 W) were considered in the model. All other boundary conditions are kept unchanged. Figure 9 shows the calculated cross-sections. While the weld seam cross-sections and the penetration depths are significantly increased in the case of a high absorption rate, the width of the weld seam is changed only slightly.

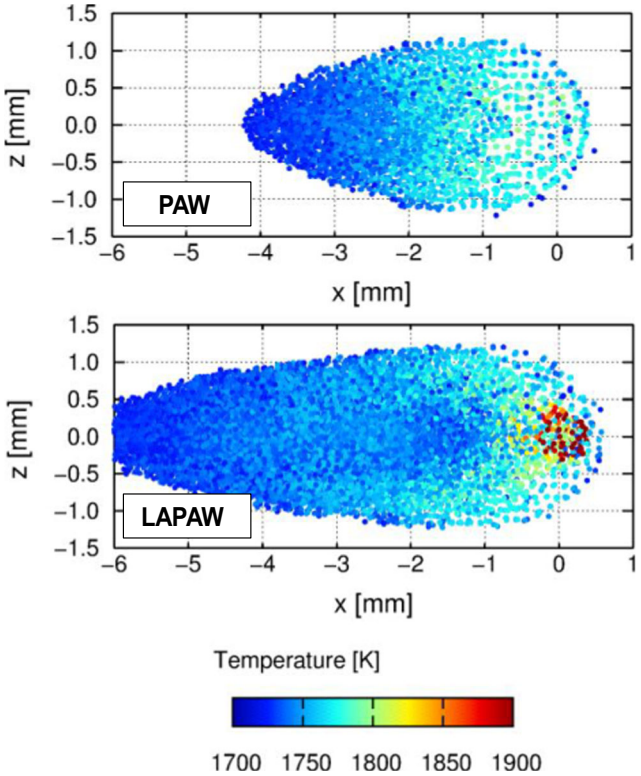

Fig. 6 Top view of the calculated temperatures in the weld pool for a PAW and a LAPAW process described in Section 2

As a result, the thermal efficiency is raised from 20% (absorption rate of 50%) to 31% (absorption rate of 100%). Because of the low thermal conductivity, the preheating of the parent material as well as the shear stresses induced by the plasma arc, the concentrated heat input of the laser is used efficiently for the melting of the parent material. In addition to

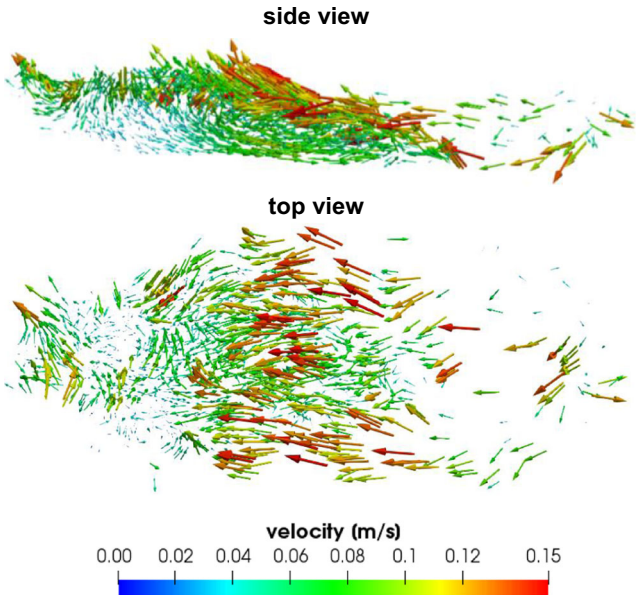

Fig. 7 Side and top view of the calculated velocity field in the weld pool for the LAPAW process described in Section 2

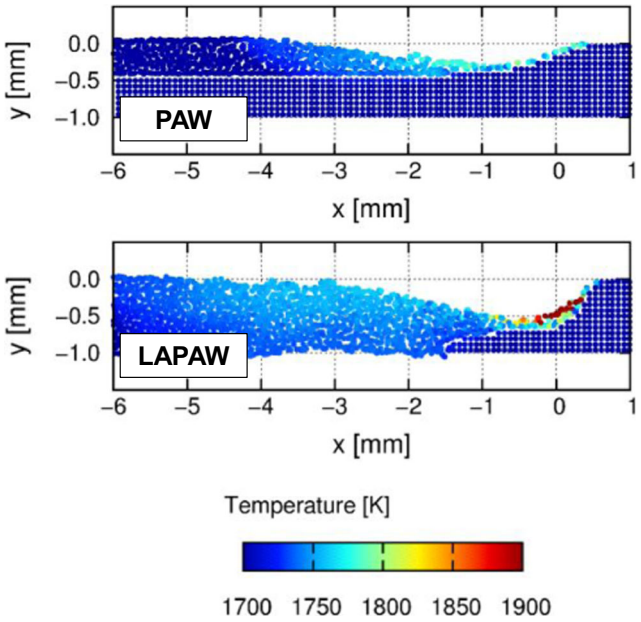

Fig. 8 Calculated temperatures in the longitudinal section for the PAW and LAPAW processes described in Section 2—the travel speed is 0.7 m/min

the increased heat input into the weld pool, the maximum temperature also increases from 1950 K (absorption rate of 50%) to 2200 K (absorption rate of 100%) (see Fig. 10). In contrast to the PAW process, a weld through could be realised in the case of an absorption rate of 100%.

The sensitive analyses suggest that a dramatically increase in thermal efficiency is primary achieved by a concentrated heat input of the laser in the weld pool.

Secondly, the influence of a laser-induced metal evaporation, which possibly causes an increased electrical conductivity and furthermore an increased heat flux density at the constricted arc root on the base material surface, is discussed. Based on the reference configuration illustrated in Fig. 4, variations of the heat flux density profile of the welding arc were considered in the model. For this purpose, the heat flux profile of the welding arc shown in Figure 4 was varied by multiplying the radius $\boldsymbol{r}$ by a factor $\boldsymbol{F_q}$ of 1.0, 1.1 and 1.2 (see Eq. 2).All other boundary conditions were kept unchanged.

$$\dot{\boldsymbol{q}}_{\boldsymbol{Arc}}(\boldsymbol{r}) = \dot{\boldsymbol{q}}_{\boldsymbol{Arc,Ref}}\left(\boldsymbol{r}\cdot\boldsymbol{F_q}\right) \tag{2}$$

In Eq. 2, $\dot{\boldsymbol{q}}_{Arc}$ is the scaled profile of the heat flux density of the welding arc used in the SPH calculation, $\dot{\boldsymbol{q}}_{Arc,Ref}$ is the heat flux density distribution of the arc process gained from the MHD-simulation, $\boldsymbol{r}$ is the radius and $\boldsymbol{F_q}$ is the scaling factor.

Consequently, the heat flux profile in the case of a factor 1.2 is more constricted compared to a factor 1.0 and 1.1. By normalising the heat flow of the arc in the model, only the heat flux density profile was changed, while the total heat input through the welding arc of 500 W could be kept constant. This

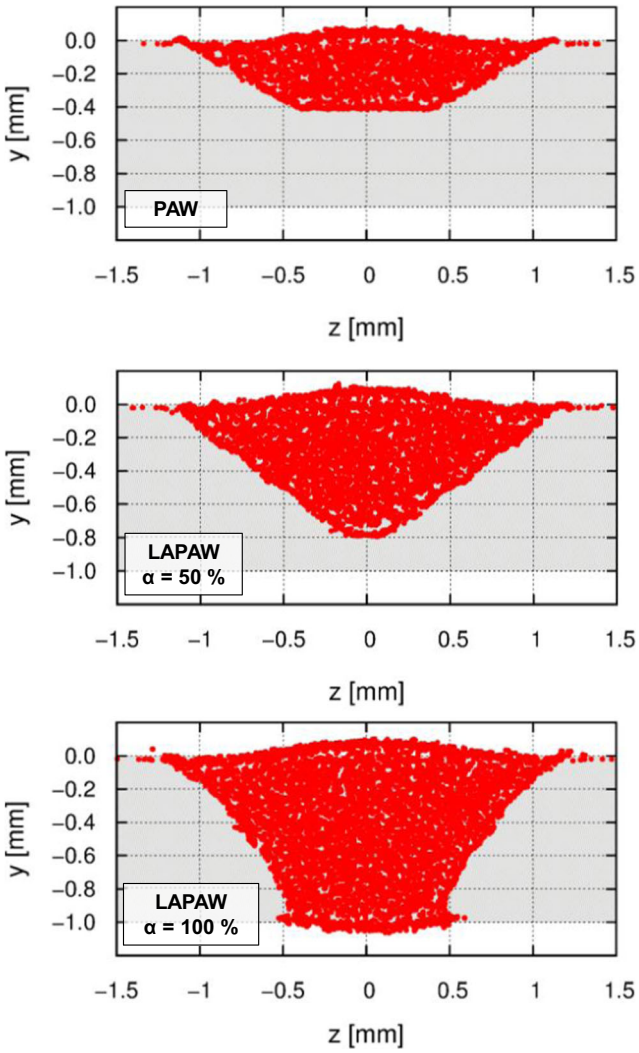

Fig. 9 Calculated cross-sections of the LAPAW process described in Section 2 for different absorption rates compared to a PAW process

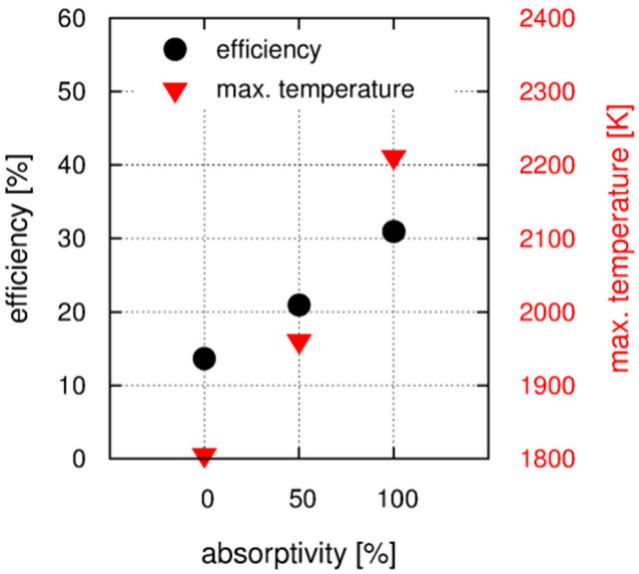

Fig. 10 Efficiency and maximum temperatures in the weld pool of the LAPAW process described in Section 2 for different laser powers

allows the influence of arc constriction to be analysed separately while keeping all other boundary conditions constant.

Figure 11 shows the calculated weld seam cross-sections of the LAPAW process with a laser power of 100 W for the different heat flux density profiles of the arc. It could be shown that a more constricted heat flux density profile of the welding arc increases the weld seem cross-section area significantly. In contrast to the reference configuration, the penetration is roughly doubled by a marginally constriction of the heat flux density profile using a factor F_q of 1.2. The weld seam width approximately stays unchanged.

Furthermore, the maximum temperatures and the thermal efficiency are increased by a constriction of the heat flux profile of the arc (see Figure 12).

Third, the influence of a possible changed flow pattern in the weld pool by the laser is discussed. However, the calculation results show that the velocity field in the weld pool does not change significantly as a result of the heat input by the laser. The velocities tend to increase with increasing laser power as the size of the weld pool increases while the temperature-dependent viscosity of the melt decreases.

A significant influence on the flow pattern of the weld pool may result from the shear stress and the stagnation pressure of the arc. In order to analyse this effect, various shear stress and stagnation pressure profiles were considered in the model. Based on the reference configuration illustrated in Fig. 4, variations of the shear stress profile of the arc were considered by multiplication of the reference profile with a factor F_S of 0, 0.5, 1, 1.5 and 2 (see Eq. 3). All other boundary conditions were kept unchanged.

$$\tau_{Arc}(r) = \tau_{Arc,Ref}(r) \cdot F_S \tag{3}$$

In Eq. 3, τ_{Arc} is the scaled profile of the shear stress of the arc used in the SPH calculation, r is the radius, $\tau_{Arc,Ref}$ is the shear stress distribution of the arc process gained from the MHD-simulation and F_S is the scaling factor.

A change of the shear stress of the arc process leads to a changed geometry of the weld pool und thus to a changed shape of the weld seam cross-section as well (see Fig. 13). An increase of the shear stress of the arc process causes an increase displacement of the melt in the front part of the weld pool. As a result, the weld pool surface deformation is enhanced. With regard to the shape of the weld seam, the penetration depth increases as well.

In addition, increasing the shear stress of the arc process leads to an increase of the flow velocities in the weld pool and thus to an intensified mixing effect within the weld pool. As a result, the temperatures are reduced (see Fig. 14). It can be concluded, that the heat induced in the workpiece by the LAPAW process is used more efficiently. This leads to

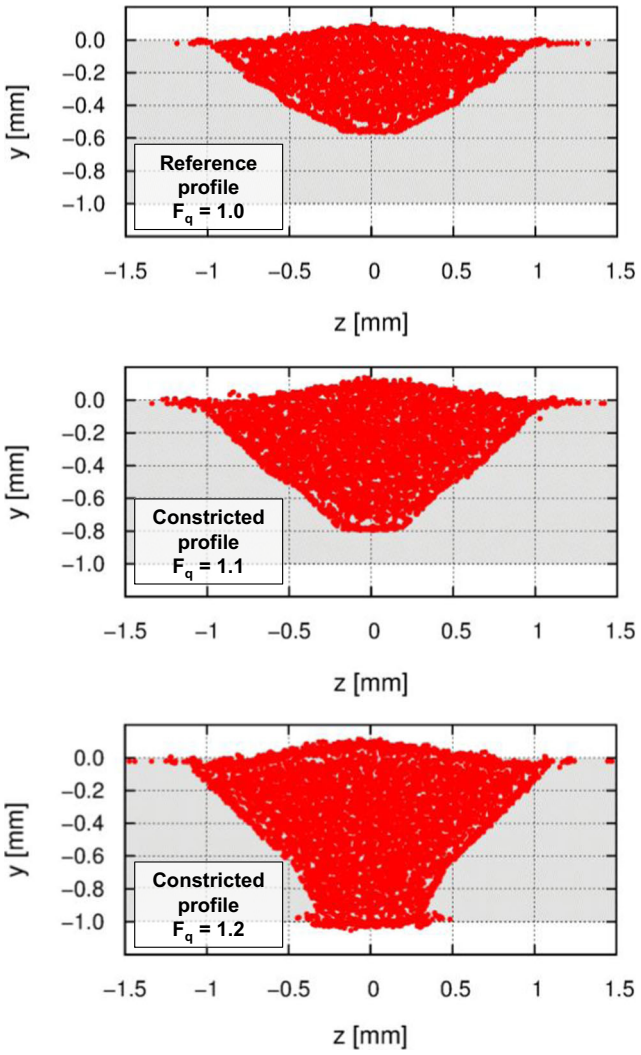

Fig. 11 Calculated cross-sections of the LAPAW process described in Section 2 for different heat flux profiles

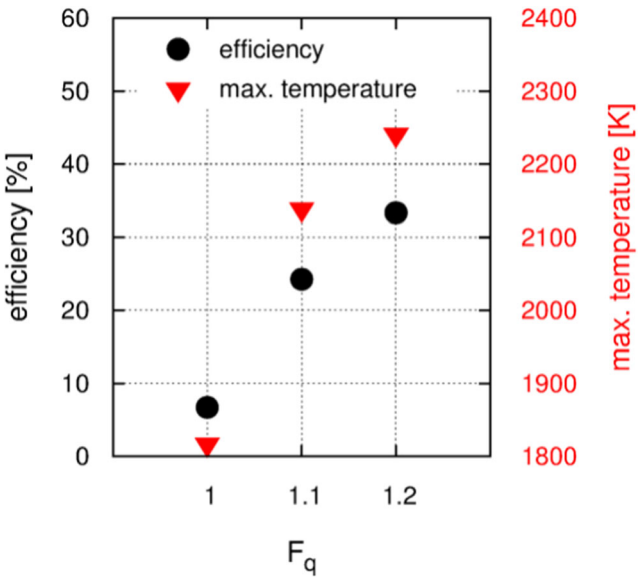

Fig. 12 Efficiency and maximum temperatures in the weld pool of the LAPAW process described in Section 2 for different heat flux profiles

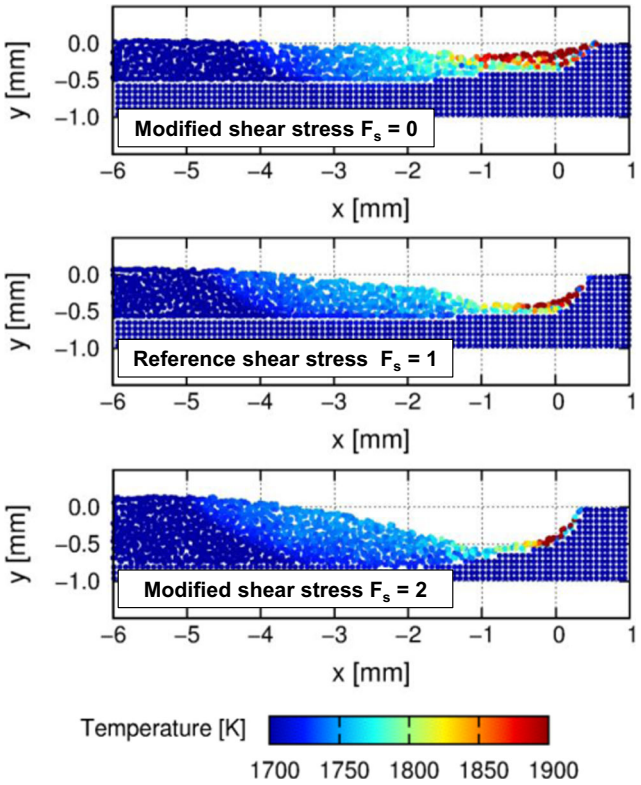

Fig. 13 Temperature distribution and weld pool deformation of the LAPAW process described in Section 2 for different shear stress profiles of the arc

enhanced weld seam cross-sections and thus to increased thermal efficiencies.

Based on the reference configuration illustrated in Fig. 4, the pressure induced by the arc process was varied by multiplication of the reference profile with a factor F_p of 0, 0.5, 1, 1.5, and 2 (Eq. 4). All other boundary conditions were kept unchanged.

$$p_{Arc}(r) = p_{Arc,Ref}(r) \cdot F_p \tag{4}$$

In Eq. 4, p_{Arc} is the scaled stagnation pressure profile used in the SPH calculation, r is the radius, $p_{Arc,\,Ref}$ is the stagnation pressure profile of the arc process gained from the MHD-simulation and F_p is the scaling factor. A change of the pressure of the PAW process results only in a slightly altered deformation of the weld pool surface in the investigated parameter range. The influence of the pressure on the temperature distribution within the weld pool and thus on the thermal efficiency of the LAPAW process is therefore negligible (see Fig. 15). However, for an arc welding process, an increase of the arc pressure is also linked to an increase of the shear stress.

6 Summary and conclusions

Numerical investigations on the synergy effect in laser-assisted plasma arc welding have been carried out. By the

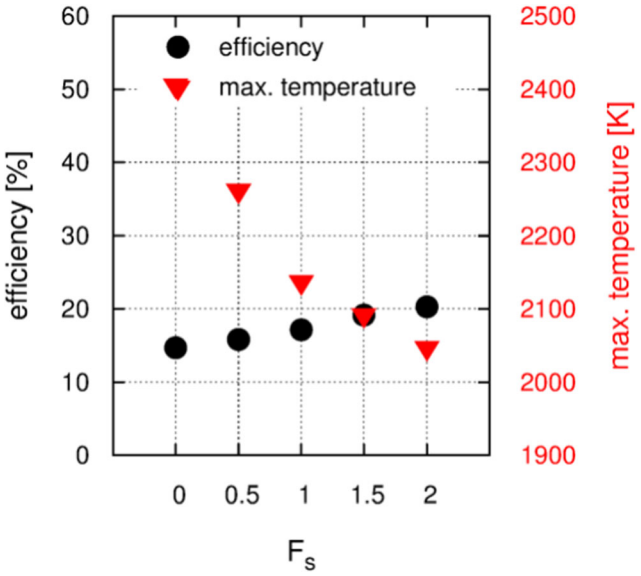

Fig. 14 Efficiency and maximum temperatures in the weld pool of the LAPAW process described in Section 2 for different shear stress profiles of the arc

use of a MHD arc model, the arc properties on the base material surface (heat flux density, stagnation pressure and shear stress) were calculated self consistently depending on the specified process parameters. The calculated arc properties and an additional heat source of the laser beam were further used in a SPH model of the weld pool. The comparison of the calculated penetration profiles with experimental determined penetration profiles shows a very good agreement for both the plasma (PAW) and the plasma-laser (LAPAW) process.

In order to quantify possible influencing factors on the synergy effect, sensitive analysis has been carried out. In the sensitivity analyses, only one parameter was changed at a time

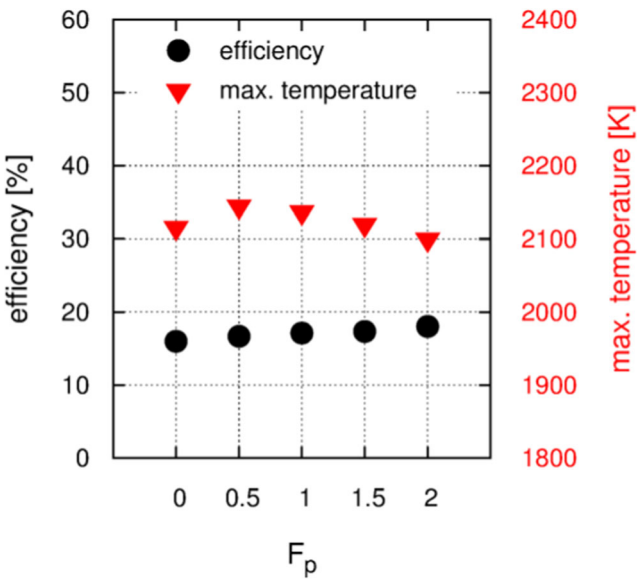

Fig. 15 Efficiency and maximum temperatures in the weld pool of the LAPAW process described in Section 2 for different arc pressures

in order to allow conclusions to be drawn about the cause and effect chains.

First, the influence of a possibly increased laser absorptivity on the base material surface has been studied. The results show a significant influence of the absorptivity on the thermal efficiency of the LAPAW process. The higher the absorption of the laser beam, the higher the penetrations depth, the thermal efficiency and the temperature in the weld pool. In comparison to a constant absorption rate of 50%, the thermal efficiency is increases from 20% up to 30% in the case of an absorption rate of 100%.

Secondly, the influence of the heat flux density of the arc was analysed. In case of an arc constriction and therefore a constriction of the heat input by the arc process, the concentrated heat input will lead to higher maximum temperatures in the weld pool, increased penetration depths as well as increased thermal efficiencies. In comparison to the calculated heat flux profile of the reference process, a constriction of heat flux profile by a radius factor of 1.2 lead to an increase of the thermal efficiency from 8 to 33%. Furthermore, the penetration is roughly doubled.

The flow field in the weld pool is marginally affected by the laser beam in the examined laser power range. The dominant driving force of the flow is the shear stress induced by the arc process. Increasing the shear stress mainly decreases the maximum temperatures in the weld pool. The influence of the stagnation pressure was negligible under the investigated boundary conditions.

The analysis clearly reveals the major influence of the central heat flux density on the penetration profile and on the thermal efficiency of the process. The higher the heat flux of the laser beam and the higher the constriction of the heat flux profile of the arc, the higher the thermal efficiency of the LAPAW process.

Funding information The authors appreciate the financial support given by the German Research Foundation (DFG) within the project "Experimentelle und theoretische Analyse des Tiefschweißeffektes beim lasergestützten Plasmaschweißen", Contract No. BE 1875/34-1 and FU 307/10-1.

Reference

1. Steen WM, Eboo M (1979) Arc-augmented laser welding. Met Constr 11(7):332–335
2. Steen WM (1980) Arc-augmented laser processing of materials. J Appl Phys 51(11):5636–5641
3. Hu B, den Ouden G (2005) Laser induced stabilisation of the welding arc. Sci Technol Weld Join 10(1):76–81
4. Stute U, Kling R, Hermsdorf J (2007) Interaction between electrical arc and Nd:YAG laser radiation. CIRP annals – manufacturing. Technology 56(1):197–200
5. Mahrle A, Rose S, Schnick M, Beyer E, Füssel U (2013) Stabilisation of plasma welding arcs by low power laser beams. Sci Technol Weld Join 18(4):323–328
6. Schnick M, Rose S, Füssel U, Mahrle A, Demuth C, Beyer E (2013) Experimental and numerical investigations of the interaction between a plasma arc and a laser. Welding in the World 56(3):93–100
7. Cui H, Decker I, Pursch H, Ruge J, Wendelstorf J, Wohlfahrt H (1992) Laserinduziertes Fokussieren des WIG-Lichtbogens, Laser induced focusing of a TIG arc, DVS Bericht, Bd. 146. DVS-Verlag GmbH, Düsseldorf (in German)
8. Decker I, Wendelstorf J, Wohlfahrt H (1995) Laserstrahl-WIG-Schweißen von Aluminiumlegierungen, Laser-TIG-welding of aluminium alloys DVS-Bericht, Bd. 170. DVS-Verlag, Düsseldorf, pp 206–208 (in German)
9. Mahrle A, Schnick M, Rose S, Demuth C, Beyer E, Füssel U (2011) Process characteristics of fibre-laser-assisted plasma arc welding. J Phys D Appl Phys 44(34):345502–345513
10. Hu B, den Ouden G (2005) Synergetic effects of hybrid laser/arc welding. Sci Technol Weld Join 10(4):427–431
11. Mahrle A, Rose S, Schnick M, Beyer E, Füssel U (2013) Laser-assisted plasma arc welding of stainless steel. J Laser Appl 25(32006–1):32006–32008
12. Mahrle A, Rose S, Beyer E, Füssel U (2014) Crucial role of beam spot position in laser assisted plasma arc welding. Sci Technol Weld Join 19(2):119–124
13. Rose S, Mahrle A, Schnick M, Pinder T, Beyer E, Füssel U (2013) Plasma welding with a superimposed coaxial fiber laser beam. Welding in the World 57(6):857–865
14. Lowke JJ, Kovitya P, Schmidt HP (1992) Theory of free-burning arc columns including the influence of the cathode. J Phys D Appl Phys 25:1600–1606
15. Tanaka M, Lowke JJ (2007) Predictions of weld pool profiles using plasma physics (Topical Review). J Phys D Appl Phys 40:R1–R23
16. Schnick M, Fuessel U, Spille-Kohoff A (2010) Numerical investigations of the influence of design parameters, gas composition and electric current in plasma arc welding (PAW), Doc. IIW-1997. Welding in the World 54(3):R87–R96
17. Gingold RA, Monaghan JJ (1977) Smoothed particle hydrodynamics - theory and application to non-spherical stars. Mon Not R Astron Soc 181:375–389
18. Ito M, Nishio Y, Izawa S, Fukunishi Y, Shigeta M (2015) Numerical simulation of joining process in a TIG welding system using incompressible SPH method. Quarterly Journal of the Japan Welding Society 33(2):34s–38s
19. Trautmann M, Hertel M, Füssel U (2017) Numerical simulation of TIG weld pool dynamics using smoothed particle hydrodynamics. Int J Heat Mass Transf 115(Part B):842–853
20. Murphy AB (2001) Thermal plasmas in gas mixtures (topical review). J Phys D Appl Phys 34(20):R151–R173
21. Cho YT, Cho WI, Na SJ (2011) Numerical analysis of hybrid plasma generated by Nd:YAG laser and gas tungsten arc. Opt Laser Technol 49:711–720
22. Kozakov R, Gött G, Uhrlandt D, Emde B, Hermsdorf J, Wesling V (2015) Study of laser radiation absorption in a TIG welding arc. Welding in the World 59:475–481
23. Radaj D (1999) Schweißprozesssimulation: Grundlagen und Anwendung. Verlag für Schweißen und verwandte Verfahren DVS-Verlag, Düsseldorf (in German)
24. Matsumoto T, Misono T, Fujii H, Nogi K (2005) Surface tension of molten stainless steels under plasma conditions. J Mater Sci 40: 2197–2200. https://doi.org/10.1007/s10853-005-1932-9